Catalysis Today 384-386 (2022) 265–273

Contents lists available at ScienceDirect

Catalysis Today

journal homepage: www.elsevier.com/locate/cattod

Segregation dynamics of a Pd-Ag surface during CO oxidation investigated by NAP-XPS

Marie D. Strømsheim [a], Ingeborg-Helene Svenum [a,b], Mehdi Mahmoodinia [a], Virgínia Boix [c], Jan Knudsen [c,d], Hilde J. Venvik [a,*]

[a] Department of Chemical Engineering, Norwegian University of Science and Technology (NTNU), NO-7491 Trondheim, Norway
[b] SINTEF Industry, P.O.Box 4760 Torgarden, NO-7465 Trondheim, Norway
[c] Division of Synchrotron Radiation Research, Department of Physics, Lund University, P.O. Box 118, SE-221 00 Lund, Sweden
[d] MAX IV Laboratory, Lund University, P.O Box 118, SE-221 00 Lund, Sweden

ARTICLE INFO

Keywords:
Palladium
Silver
Segregation
Single crystal surface
Bimetallic catalysis
Carbon monoxide oxidation

ABSTRACT

The dynamic changes in composition in the near-surface region of a $Pd_{75\%}Ag_{25\%}(100)$ single crystal were monitored using near-ambient pressure x-ray photoelectron spectroscopy (NAP-XPS) during CO oxidation under oxygen rich conditions at a total pressure of 1.1 mbar. Six CO oxidation temperature cycles were investigated at different heating rates and maximum temperatures of 450 °C or 600 °C. It was found that the history of the bimetallic sample plays an important role, as the CO_2 formation profile varies depending on initial conditions, and previous heating rates and maximum temperatures. In terms of CO coverage effects, normal, reversed and no hysteresis behaviour were all observed. In agreement with previous modelling predictions, the NAP-XPS data confirm a dynamic segregation behaviour upon heating/cooling where the amount of Pd in the surface region decreases with increasing temperature. Nevertheless, the Pd $3d_{5/2}$ core level relative area assessment is not fully capable of capturing all the surface dynamics inferred from the temperature dependent CO_2 formation profiles, due to the probing depth. While residing at ambient temperature in the reaction mixture, however, there is a build-up of adsorbed CO at the surface showing that CO induces segregation of Pd to the topmost surface layer under these conditions. In total, this suggests that the segregation is kinetically relatively facile during temperature cycling, and that adsorbate coverage is the main controlling factor for the surface termination.

1. Introduction

Bimetallic catalysts are widely studied in chemical conversion. The motivation behind the alloying may be either promoting effects (activity, selectivity or stability) or cost saving, i.e. replacing a portion of a scarce and expensive platinum group metal (PGM) with a cheaper element while maintaining the overall properties. During the last decades, the possibility of combining only less costly and abundant elements to obtain PGM replacements has also been facilitated by the development in computational methods and high throughput experimentation [1,2]. In the context of bimetallics, it is important to establish to what extent the surface composition of a nanoparticle or crystal surface is controllable or purely determined by the reaction conditions. It is easy to predict that chemical bonds to adsorbed species will affect the energetically favourable termination of an alloy [3–5], in addition to the energetics of the alloying elements themselves. The latter was systematically discussed in a much-cited theoretical investigation by the Nørskov group [6]. In addition, highly relevant to thermochemical processes, the temperature will affect the termination both thermodynamically and kinetically. Hence, segregation may be induced upon change in partial pressure and/or temperature.

X-ray photoelectron spectroscopy (XPS) is a suitable characterization technique to study segregation and it is widely used due to its elemental and chemical sensitivity. The majority of XPS studies have been performed in high-vacuum or ultra-high vacuum (UHV); partly to avoid scattering of photoelectrons in the gas and partly because the detector requires high vacuum. Stepwise developments to the instrumentation (accelerators, monochromators, detectors, differentially pumped electron analysers, etc.) over several decades, however, now allow surface characterization under higher pressure, see [7,8] and references cited therein. The technique may then be referred to as near-ambient pressure XPS (NAP-XPS) and offers the possibility of studying catalysts or

* Corresponding author.
E-mail address: hilde.j.venvik@ntnu.no (H.J. Venvik).

https://doi.org/10.1016/j.cattod.2021.02.007
Received 1 December 2020; Received in revised form 29 January 2021; Accepted 17 February 2021
Available online 26 February 2021

catalytic model systems under working conditions. Dedicated NAP-XPS beamlines are today found at many synchrotron sources capable of characterising catalysts at temperatures from room temperature to 600−700 °C and from UHV to 20−30 mbar [8]. In addition, there are NAP-XPS systems that use conventional x-ray sources [9], albeit some limitations and constraints relative to the synchrotron-based experiments. Reactant and product analysis is usually also possible, with mass spectroscopy being utilized the most. The current work seeks to experimentally study the segregation behaviour of an alloy model catalyst through the use of NAP-XPS.

The catalyst model system applied here is a $Pd_{75\%}Ag_{25\%}(100)$ alloy single crystal. Palladium is a widely applied catalyst within the PGM group, with excellent properties in oxidation [10] as well as hydrogenation/dehydrogenations reactions [11–18]. Pd nanoparticles assist the oxidation of CO and hydrocarbons in automotive catalysis [19,20], and since both the metal and the oxide exhibit activity, the chemical state of the Pd surface in oxidation reactions has been much scrutinized. Moreover, model system (single crystal) investigations have disclosed a range of (active) surface oxides [21–30], as defined as ordered Pd-O structures of 1–3 atomic layers residing on top of the metallic fcc lattice. However, Pd is expensive and scarce, and high dispersion is often critical to the commercial application. Either low temperature activity (<300 °C) or high temperature stability (> 800 °C) is commonly desired for Pd applications in oxidation catalysis. In other applications, if for example 25 % of the Pd could be replaced without compromising on other properties, it would still be attractive. This applies to some extent for PdAg based hydrogen membrane technology, although there are also beneficial effects with respect to stability and hydrogen diffusivity [32]. Another example is the case of hydrogenation, where alloying with Ag moderates the reaction, thereby increasing the yield of alkene versus alkane and suppressing carbon formation [12–15,18]. Silver may not be the obvious candidate for enhancing the low temperature activity of Pd towards oxidation, but its complex properties in oxidation catalysis makes it an interesting alloying element [31]. To control properties of bimetallic systems, the alloying and segregation behaviour in response to variations in the reaction conditions should be understood and described, in particular their impact to the surface termination, here Pd versus Ag.

While $Pd_{75\%}Ag_{25\%}(100)$ is our model catalyst, CO oxidation is used as a reaction probe. The high turnover rates and simple reactant/product mixture composition lend it readily to NAP-XPS single crystal investigations. It is also much studied over different Pd surface terminations and in relation to metallic and (surface) oxidic states. We have made two preceding investigations, involving either Ag [33] or Au [34] as alloying elements to Pd. Here, it was found that while Pd_3Au (100) behaves relatively similar to pure Pd(100), $Pd_{75\%}Ag_{25\%}(100)$ displays some clear differences. The first concerns the ordered $(\sqrt{5}x\sqrt{5})R27^\circ$ surface oxide (hereafter termed as $\sqrt{5}$) that is present on Pd(100) and $Pd_3Au(100)$ under O_2:CO = 10:1 mixtures in the high activity regime (light-off >190 °C), while this is not the case for $Pd_{75\%}Ag_{25\%}(100)$. This surface oxide has been shown to form, however, on all three surfaces in pure O_2 in the sub-millibar regime and at temperatures of 300−320 °C [33–35]. The second difference concerns the activity hysteresis prevailing due to CO coverage effects. On Pd(100) and $Pd_3Au(100)$, we find the "normal" hysteresis, in which removal of an inhibiting CO coverage requires higher temperature while heating than establishing the same CO coverage while cooling. This behaviour is reversed for $Pd_{75\%}Ag_{25\%}(100)$. A schematic for the normal and reversed hystereses is displayed in Fig. 1. Based on combined first principles and microkinetic modelling the reversed hysteresis observed for $Pd_{75\%}Ag_{25\%}(100)$ could be attributed to combined effects of segregation and coverage during temperature cycling. In more detail, the prediction may be understood as follows: In absence of adsorbates (vacuum) the surface of a PdAg- alloy will be Ag-rich [3,4,36,37], as Ag has a lower surface energy than Pd [38] and slightly larger atomic radius than Pd. Then, almost any chemisorbed species (e.g. oxygen, CO and hydrogen)

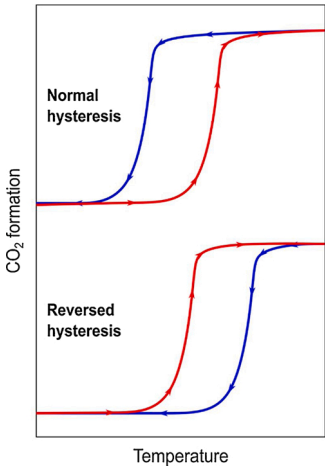

Fig. 1. Schematics for the normal and reversed hystereses for CO_2 formation as a function of temperature. Red colour indicates increasing temperature, and blue colour indicates decrease in temperature.

will preferentially bind to Pd and induce a driving force for segregation of Pd to the surface [3,4,35,36,39]. Such segregation will be kinetically facilitated by temperature, but at high temperature the coverage is reduced to an extent that promotes reversed segregation (Ag to the surface) [33]. This proceeds as the temperature is increased, and a low fraction of Pd in the surface is established. Upon cooling the low amount of Pd in the surface is incapable of maintaining a high reactant coverage and the same high rate as upon increase, and extinction therefore occurs at higher temperature than ignition.

Our previous work on the $Pd_{75\%}Ag_{25\%}(100)$ was focused on the comparison of its activity with respect to pure Pd(100) and the absence of the surface oxide. No efforts to determine the relative distribution of Ag and Pd in the near surface region were, however, made in this study and direct experimental evidence for the segregation model explaining the reversed hysteresis is therefore still missing. In the present work we give this evidence. Moreover, we seek to establish methodology for investigating the dynamics of segregation phenomena over different temperature ranges and heating/cooling rates. This requires good temperature control while at the same time following the relevant core levels of the alloying element under reactant mixture exposure, and this fits well with the capabilities of the HIPPIE beamline at the MAX IV Laboratory.

2. Materials and methods

The NAP-XPS measurements were carried out at the HIPPIE beamline [8] at the MAX IV Laboratory. A schematic of the end-station with the ambient pressure cell (AP-cell) [40], used as a reactor with the sample installed, and hemispherical electron analyser with differential pumping is illustrated in Fig. 2a. This setup allows NAP-XPS measurements in gas mixtures with a pressure up to about 30 mbar. Before data acquisition, the sample is placed in the AP-cell equipped with a 300 μm aperture and with a sample-aperture distance of ~0.6 mm. This sample-aperture distance ensures unaffected pressure on the sample by the nearby and differentially pumped aperture, while simultaneously minimizing the distance the photoelectrons have to travel within mbar gas pressures [41]. Heating is performed by directing a laser towards the back side of the sample, and temperatures up to 600 °C can be reached. The gas composition can be monitored at three different locations using a mass spectrometer: at the gas supply inlet, outlet or above the sample via the analyser cone. An example of how the Pd 3d and Ag 3d core level binding energies change upon heating in a CO + O_2 environment together with changes in the CO_2 partial pressure are shown in Fig. 2b. It is important to note that NAP-XPS results are sensitive to the

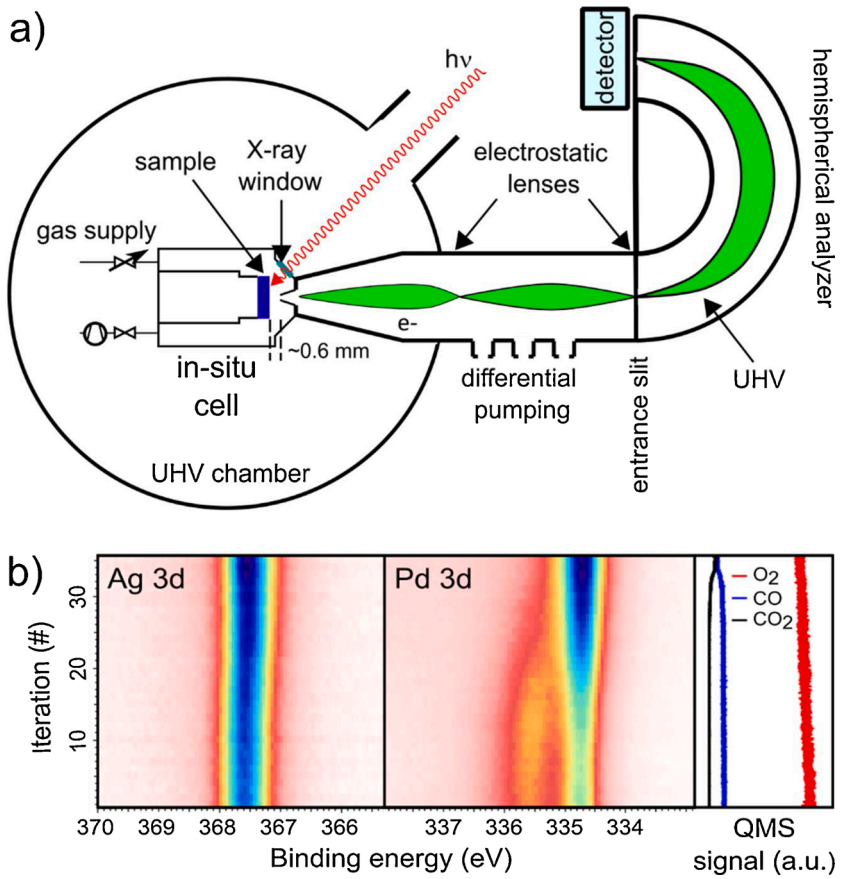

Fig. 2. a) Illustration of the NAP-XPS experimental setup with the in situ reaction cell, hemispherical analyzer and differential pumping system. b) Example of NAP-XPS spectra of the Ag 3d and Pd 3d core level regions acquired continuously under CO oxidation during heating from ~30 °C to ~290 °C together with the corresponding QMS data.

experimental setup as previously shown for CO oxidation experiments [24]. This sensitivity stems from the mass transfer limitations resulting from the geometry of the experimental cell and the sample (flat surface) in conjunction with the high activity of CO oxidation over Pd-based catalysts. This is important to keep in mind when comparing NAP-XPS results obtained using different experimental setups.

The $Pd_{75\%}Ag_{25\%}(100)$ single crystal was mounted on a 304 L steel plate and fastened by 304 L steel clips. The temperature was measured with a K-type thermocouple spot-welded to the side of the crystal. The crystal was cleaned by standard cycles of argon sputtering with subsequent annealing in oxygen (p_{O2} ~$1{\cdot}10^{-7}$ mbar) at 450–540 °C. The cleanliness of the crystal was verified by survey scans where no additional elements besides Pd and Ag were observed. Relevant core level regions were acquired with the following photon energies: O 1s at 650 eV, Pd and Ag 3d at 450 eV, and C 1s at 390 eV. All spectra were measured at normal emission, and calibrated to the Fermi edge, which was recorded immediately after acquiring the corresponding core level region. With a photon energy of 450 eV, the inelastic mean free path is 4.13 Å for Pd and Ag, found by the QUASES-IMFP-TPP2M program [42] using the Tanuma, Powell and Penn algorithm [43]. The sampling depth is about 6 atomic layers if considering that 95 % of the detected signal originates within this depth [44]. It should be noted that the signal intensity is highest for the topmost surface layer and decreases for the underlying layers.

CO oxidation was performed feeding 0.45 Nml/min CO and 4.54 Nml/min O_2, and the total pressure in the cell was ~1.1 mbar. Six CO oxidation cycles were run, three to 450 °C at 0.1 °C/s heating/cooling rate and three to 600 °C at 0.2 °C/s and 0.4 °C/s. The gas composition was monitored by QMS via the analyser cone, i.e. close to the sample surface. The pressure was measured at the outlet of the cell due to a defective in situ gauge at the beamtime, and no further calibration procedures were applied. As we actively pump on this line the real pressure in the cell could be 10–20 % higher. The QMS signal and temperature were recorded separately and the CO_2 QMS signal was time-correlated and plotted against temperature using Python. The noise was reduced by applying Savitzky-Golay filter where the length of the filter window was set to 15 and a second order polynomial was applied. In order to investigate the ratio of Ag and Pd, the Ag and Pd 3d core levels were monitored consecutively during four of the CO oxidation cycles (see Fig. 2), i.e. continuously switching between recording the Ag 3d and Pd 3d core level regions. In addition, the O 1s core level region was monitored in two of the CO oxidations cycles, to follow surface and gas phase oxygen species. Note that it was not possible to follow all three regions in the same cycle due to the different photon energies required. The O 1s region must be acquired at photon energies well above the binding energies of oxygen components typically probed in the region 528–533 eV, and here we used 650 eV. The Ag and Pd 3d core levels could be recorded at this photon energy, however, with a significant loss of surface sensitivity. A lower photon energy of 450 eV, also a compromise against the cross section of the scattering and the performance of the monochromator, was therefore chosen.

Fitting of the acquired core level spectra was performed using Doniach-Šunjić lineshape [45] convoluted with a Gaussian line shape and applying a linear background. This line shape is commonly applied for fitting of the Pd 3d core level of Pd and Pd-based single crystals [24,33,35,46,47]. The spectra were normalized with respect to the low binding energy side, unless otherwise stated. Asymmetry parameters were added to the Pd and Ag bulk and surface components. The relative amount of Pd in the near-surface region was calculated as the total area of Pd $3d_{5/2}$ relative to the total area of the Pd $3d_{5/2}$ and Ag $3d_{5/2}$ spectra.

Correspondingly, the relative amount of Pd bound to CO was calculated as the area of the CO-induced peaks in the Pd $3d_{5/2}$ spectra relative to the total area of Pd $3d_{5/2}$ and Ag $3d_{5/2}$. The areas were corrected with cross sections [48] of 4.05 and 3.86 for Ag 3d and Pd 3d, respectively. The fitting was performed in Igor Pro, version 8, from Wavemetrics Incorporated [49]. Details regarding the fitting parameters are given in Table S1 and S2 of the Supplementary Information.

3. Results and discussion

3.1. CO oxidation over $Pd_{75\%}Ag_{25\%}(100)$

CO_2 formation profiles as a function of temperature for the six CO oxidation cycles investigated over $Pd_{75\%}Ag_{25\%}(100)$ under oxygen rich conditions are shown in Fig. 3 (O_2:CO = 10:1 and ~1.1 mbar total pressure). The first three cycles (Fig. 3a–c) were performed by ramping the temperature from room temperature with a heating rate of 0.1 °C/s reaching the maximum temperature of 450 °C, with subsequent cooling down to the initial temperature at the same rate. The 4th, 5th and 6th cycles (Fig. 3d–f) had a rate of 0.2, 0.4 and 0.4 °C/s, respectively, and a maximum temperature of 600 °C. Prior to the first cycle, the sample was oxidized in O_2 at 1.1 mbar at temperatures up to 150 °C, leaving a rather thick, bulk-like palladium oxide at the surface (not shown). PdO is also known as active, but the layer is readily reduced under the reactant mixture as the temperature increases, confirmed by the disappearance of a bulk oxide contribution in Pd 3d (not shown) [29]. As shown in Fig. 3a, the light-off occurs at ~275 °C (determined at the temperature when the CO_2 formation reaches 3/4 of a noise averaged maximum production). The extinction occurs at a slightly lower temperature, ~270 °C. With a slightly higher light-off temperature than extinction temperature the hysteresis is normal for the 1st reaction cycle (Fig. 3a) in contrast to the previously reported reversed hysteresis for $Pd_{75\%}Ag_{25\%}(100)$ [33]. This is likely due to the initial palladium oxide layer prior to the 1st heating rendering a Pd rich surface.

The 2nd and 3rd cycles (Fig. 3b and c) both have a distinct increase in the CO_2 formation upon heating at temperatures around 270 °C, and the subsequent reduction in CO_2 formation occurring at a higher temperature of about 280 °C, i.e a reversed hysteresis. The 4th cycle (Fig. 3d) also exhibits a reversed hysteresis. However, although the CO_2 formation resembles that of the 2nd and 3rd cycles upon heating, a notable change can be observed during cooling from 600 °C. This is after having reached this temperature under reaction conditions for the first time. Furthermore, after reaching the maximum temperature, the conditions were maintained for roughly 50 min. for additional characterization (typically, additional core levels). The reduction in CO_2 formation now starts at higher temperature (~350 °C) and with a considerably lower slope compared to the previous cycles. Continuing to the 5th cycle (Fig. 3e), the heating as well as the cooling sections of the curve display lower slopes than the 1st – 3rd cycles, albeit still consistent with a reverse hysteresis. The heating and cooling section of the 6th cycle (Fig. 3f) are, however, nearly identical. The fact that the hysteresis change as function cycle number and in particular the first time a heating-cooling cycle is performed to a higher temperature suggests that segregation changes the surface composition with time. To verify this, the NAP-XPS data measured simultaneously as the CO_2 formation profiles were analysed.

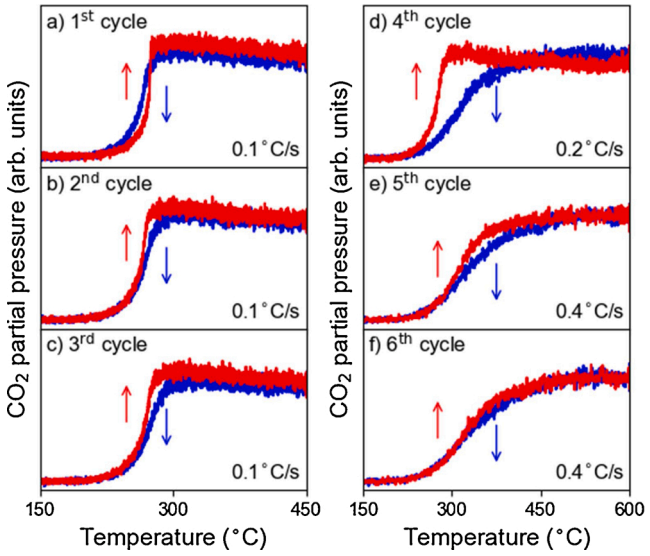

Fig. 3. CO_2 formation over $Pd_{75\%}Ag_{25\%}(100)$ measured by QMS as function of sample temperature for six consecutive reaction cycles under O_2:CO=10 and ~1.1 mbar total pressure. Red curves represent heating and blue curves the subsequent cooling. Cycles 1-3 were made with 450 °C (left panel, a-c) and cycles 4-6 with 600 °C (right panel, d-f) maximum temperature. The corresponding heating rates in the range 0.1-0.4 °C/s are indicated.

Fig. 4 shows the in situ NAP-XPS measurements during the 4th CO oxidation cycle, where there is a large change in the CO_2 formation profiles upon heating versus cooling as shown in Fig. 3d. The Ag $3d_{5/2}$ and Pd $3d_{5/2}$ core level regions were continuously acquired (live spectra in lower panel of Fig. 4) as the temperature was ramped with 0.2 °C/s up to the maximum temperature of 600 °C and down to ambient temperature again with the same rate. Selected spectra at different temperatures in the heating and cooling series are included in the upper part of Fig. 4 to better visualize the main changes occurring.

At the beginning of the heating series (Fig. 4, left panels), the Pd $3d_{5/2}$ spectrum displays one component representative of the bulk of the alloy (334.7 eV, blue) and additional contributions shifted to higher binding energy that originate from Pd bound CO. The fitting of the latter is consistent with the presence of two different CO species at binding energies of 335.6 eV (light green) and 336.2 eV (dark green). Previously, only one rather broad contribution at 335.8 eV was reported due to CO on $Pd_{75\%}Ag_{25\%}(100)$ [33], possibly covering both the CO induced contributions observed here. It was also shown that the coverage of CO obtained on $Pd_{75\%}Ag_{25\%}(100)$ was lower compared to Pd(100) and this was attributed to the presence of Ag in the topmost surface layer [33]. CO occupies Pd-Pd bridge sites on Pd(100) and two peaks associated with CO in bridge sites can be observed in the Pd $3d_{5/2}$ core level region, depending on coverage [50]. The two contributions at binding energies 335.5 eV and 335.9 eV arise due to Pd coordinated to one or two CO molecules, where the latter is observed at a CO coverage of 2/3 monolayer (ML) [23,50,51]. Minor amounts of CO occupying Pd top sites have been observed upon increasing the pressure to ~0.7 mbar [52]. CO in top site was observed for $Pd_3Au(111)$, where linearly bonded CO gave rise to a shift of +0.38 eV in Pd 3d towards higher binding energy compared to CO situated in bridge sites [53]. Based on comparison with Pd(100) and $Pd_3Au(111)$, it is likely that the CO induced components obtained here are caused by bridge (335.6 eV) and top-bonded (336.2 eV) CO on Pd75 %Ag25 %(100), the latter possibly enhanced by the alloying (Ag or Au).

The Ag $3d_{5/2}$ spectrum of Fig. 4 at room temperature can be fitted with two peaks, a major contribution at 367.7 eV (light blue) binding energy and a minor peak at 367.4 eV (red). The spectrum 1 (left panel) bears strong resemblance to the Ag $3d_{5/2}$ presented for the clean surface in a previous investigation of $Pd_{75\%}Ag_{25\%}(100)$, in which these were attributed surface Ag and Ag in the bulk of $Pd_{75\%}Ag_{25\%}(100)$, respectively [35]. A similar interpretation here infers significant amount of surface Ag and little in the bulk within the probe depth. But, since we start with PdO and also observe considerable contributions consistent with CO adsorbed on Pd, we think that the main contribution could originate from Ag rich environments both near and in the top layer. Ag $3d_{5/2}$ in pure Ag is found at slightly higher binding energy (368.15 eV) [31] whereas interaction with oxygen [31,54] or increasing contents of Pd (in nanoparticles) [55] also have been shown to shift the binding

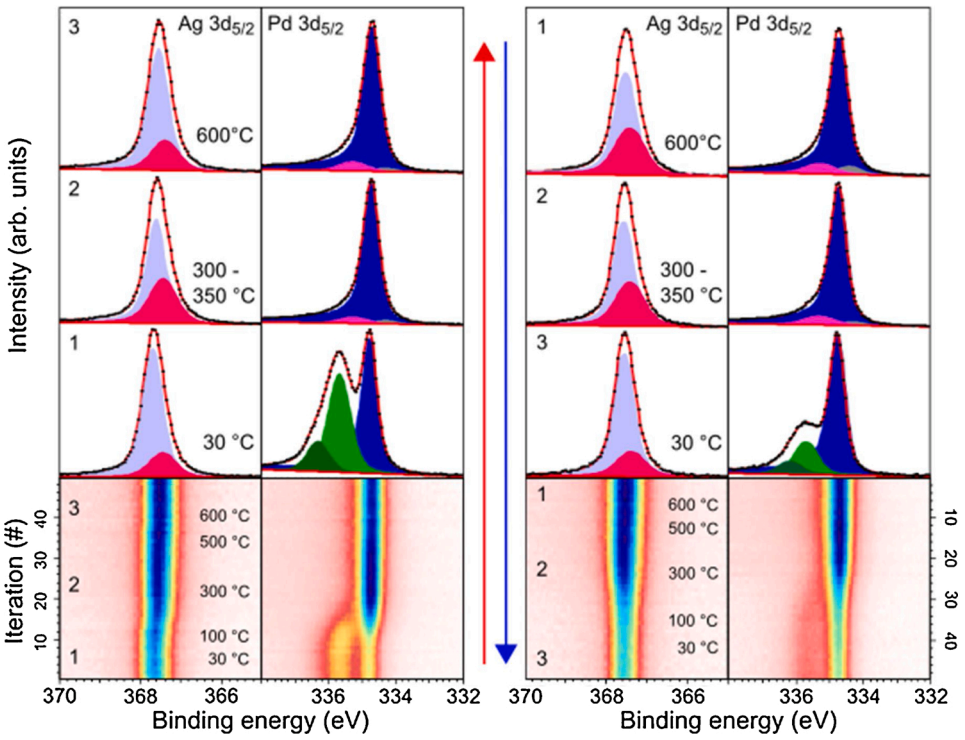

Fig. 4. Ag $3d_{5/2}$ and Pd $3d_{5/2}$ core levels recorded using a photon energy of 450 eV during CO oxidation over $Pd_{75\%}Ag_{25\%}(100)$ for the 4th reaction cycle, during heating to 600 °C (left) followed by cooling (right). Lower panels show the live spectra as a function of temperature, upper panels show selected spectra with fitted components extracted at the temperatures of interest (indicated with 1-3 in the lower panels); at close to room temperature, 300-350 °C, and 600 °C. O_2:CO=10 and ~1.1 mbar total pressure, 0.2 °C/s heating rate. The spectra in the upper panels were normalized with respect to the high intensity peak.

energy to lower values. It should also be kept in mind that Fig. 4 should not be directly used to compare ratios of Ag versus Pd, since the spectra have been normalized with respect to the high intensity contributrion. The ratios will be further analysed below.

Upon heating to ~250 °C, the CO components in Pd $3d_{5/2}$ disappear and there is a slight change in the Ag $3d_{5/2}$ in situ spectrum. This point corresponds to light-off as observed in Fig. 3d. The Pd 3d spectra recorded at 300−350 °C display mainly the Pd bulk component at 334.7 eV (blue), and then two minor components at 335.3 eV (pink) and 334.2 eV (grey) in addition. The one at 335.3 eV can be caused by Pd bonded to oxygen or Pd embedded in a Ag-rich top layer, and the other to surface Pd [33,35,46]. The Ag $3d_{5/2}$ spectra recorded at similar temperature display the same peaks as found at lower temperature, but with a change in their relative ratios. The main Ag $3d_{5/2}$ component decreases and the contribution at lower binding energy increases. No significant changes in Pd $3d_{5/2}$ are observed upon further heating to the maximum temperature of 600 °C. With respect to Ag $3d_{5/2}$, the main component again slightly increases and the contribution at lower binding energy decreases, i.e. there is no consistent trend with temperature and the changes are difficult to fully rationalise. But if the minority component is associated with Ag interacting with O, it could make sense that such interaction is to some extent favoured at intermediate temperature where surface Pd facilitates O_2 activation and the sticking is appreciable.

The subsequent cooling series is displayed in the right panels of Fig. 4. At the beginning, having maintained the reaction conditions at 600 °C for about 50 min, changes have occurred in the spectra. The minor Ag $3d_{5/2}$ component has again increased relative to the major Ag component. This could be consistent with, albeit lower sticking at high temperature, an increasing contribution from more Ag-rich regions interacting with O. The corresponding Pd $3d_{5/2}$ spectrum is less changed, but the component associated with Pd surface atoms appears slightly higher compared to the bulk and Pd-O components, possibly consistent with generally low coverage. After cooling to 300−350 °C, the development in the Ag $3d_{5/2}$ component at lower binding energy could be explained by less Pd-assisted O_2 activation. Minor changes are found in the Pd $3d_{5/2}$ spectra, possibly due to the main part of the signal originating from Pd beneath the topmost layer. Lowering the temperature below ~250 °C again yields a CO induced component in the Pd $3d_{5/2}$ core level spectra that continues to grow as the temperature approaches 30 °C, signifying segregation of Pd to the topmost layer. The contributions induced by CO in Pd $3d_{5/2}$ is smaller than at the start of the series, implying that more Ag is still present in the topmost layer, and this behaviour will be further analysed below.

The discussion above shows that there is no simple explanation or clear trend in the fitted Ag $3d_{5/2}$ and Pd $3d_{5/2}$ core level components as function of temperature for a single cycle, except that of CO adsorbed. Extensive experimentation and modelling may be needed to uniquely explain all the fits, but the remaining discussion focusses on what can be extracted from the existing data.

3.2. *Segregation in the near-surface region during CO oxidation temperature cycling*

The Ag $3d_{5/2}$ and Pd $3d_{5/2}$ core levels acquired during the CO oxidation cycles can also provide insight into the change in the relative amount of Pd in the near-surface region. The ratio of Pd to total metal for the 1st, 2nd, 4th and 5th CO oxidation cycles is shown in Fig. 5. It should be noted that each point in the curve is based on a single sweep from the in situ measurements of Ag $3d_{5/2}$ and Pd $3d_{5/2}$ core levels, and this results in relatively poor signal-to-noise ratio. It should also be kept in mind that the depth probed is several atomic layers, with gradually reducing relative contributions from each layer. The exact surface composition is hence blurred by the composition of sub-layers and the distribution between all the probed layers. Despite these limitations, it is worth to discuss the overall trends. The first cycle starts with the highest relative amount, 0.73, and this is due to the pre-oxidation to form a bulk-like PdO layer as described above. The estimated Pd concentration first decreases with temperature before increasing towards 450 °C. Then, the relative amount of Pd reduces while maintaining (again for characterization purposes) reaction conditions at 450 °C before slightly increasing upon reducing the temperature. After one full cycle the amount of Pd in the surface region ends up at a lower level, ~0.65. In contrast, the estimated ratios in the 2nd cycle show no increase or decrease as the temperature is ramped up and down. This could indicate that the

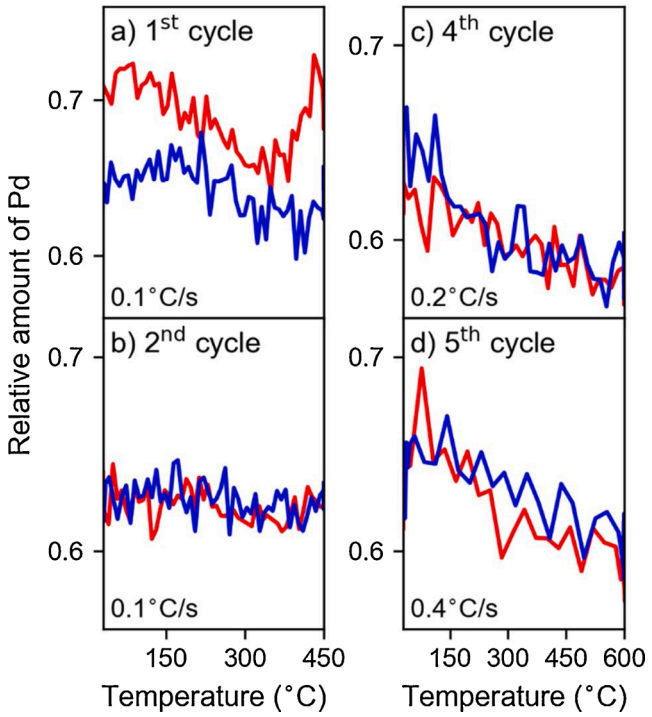

Fig. 5. Relative amount of Pd in comparison to the total amount of Ag and Pd in the probed layers of $Pd_{75\%}Ag_{25\%}(100)$ as function of sample temperature under O_2:CO=10 and ~1.1 mbar total pressure. Red curves represent heating and blue curves the subsequent cooling. Cycles 1-2 were made with 450 °C (left panel, a-b), and cycles 4-5 with 600 °C (right panel, c-d) maximum temperature. The corresponding heating rates in the range 0.1-0.4 °C/s are indicated.

redistribution between Pd and Ag within the probed layers is not prominent, likewise the exchange with the bulk, in this range of temperature. Nevertheless, the reversed hysteresis in the reaction data (Fig. 3b-c) suggest that there are changes in the surface layer composition. It could be that these changes mainly occur within the 2–3 outmost layers.

The fourth cycle is the first cycle for which the maximum/end temperature and rate were increased. The relative amount of Pd decreases from ~0.63 at room temperature to ~0.57 at 600 °C, and subsequently decreases to roughly the same level as the temperature goes down. The same trend and similar values are found for the fifth cycle, which had the same setpoint temperature, but a higher rate of 0.4 °C/s. These results indicate that the segregation kinetics are to a certain degree facile within the probed layers across the temperature range, in partial contrast to the cycles 1–2. The temperature dependency of the CO_2 formation changes significantly, however, especially for cycle 4 where an increase in temperature from the previous cycles resulted in a marked change in the hysteresis curve (Fig. 3). This suggests that compositional changes beyond those captured by the ratio estimates take place, as for the first two cycles. Theoretical calculations indicated that the interface between the surface oxide and bulk structure on Pd75 %Ag25 %(100) consists of a silver rich layer [35], and the situation might be similar for a CO covered surface. An enrichment of Ag directly beneath the topmost surface layer is a possible explanation for the changes observed in the hysteresis curves (Fig. 3).

In summary, we may conclude that segregation phenomena do take place and can be accounted for by assessing the relative amount of Pd. The constraints on probe depth in the applied setup make it difficult to capture the full segregation dynamics. Reducing the probe depth through a lower photon energy (e.g. 410 eV for Pd 3d) was not a practical solution at the applied setup due to a reduced intensity and higher level of background in comparison to 450 eV, and using 400 eV was not possible because of the x-ray windows. Furthermore, there is a significant reduction in cross section for Ag 3d at 410 eV compared to 450 eV. Applying two different photon energies throughout the in situ measurements of core levels Ag 3d and Pd 3d was also not feasible, and neither is it possible to apply a grazing angle in the applied reaction cell.

3.3. Changes in the composition of the topmost layer determined by adsorbed CO

Although it was not possible to adjust the surface sensitivity further, the amount of CO present on the surface provides a measure of the amount of Pd in the top layer since CO will preferentially adsorb on Pd and not Ag [56–61]. As discussed in section 3.1, the Pd $3d_{5/2}$ core level at ambient temperature contains contributions from Pd in the bulk and CO-induced peaks, i.e., a shift in binding energy due to CO adsorbed on Pd. These latter contributions can be used as another way of assessing the exchange of Pd to and from the topmost surface layer.

The fraction of surface Pd bonded to CO was estimated through fitting each sweep of the Pd $3d_{5/2}$ live spectra (Fig. 4) in the temperature range where the CO coverage is appreciable (ambient temperature to ~250 °C). Fig. 6 shows the relative amount of CO bonded to Pd for the 2nd, 4th and 5th cycle, and the corresponding Pd $3d_{5/2}$ spectra at room temperature at the beginning and end of these cycles are shown in Fig. 7. Fig. 6 shows that the relative amount of Pd bound to CO during heating and cooling, varies in the range 0.12 to 0.34 at ambient temperature, and 0.04−0.10 at 250 °C. It should be kept in mind, however, that this relative amount also reduces due to CO desorption at increased temperature. Moreover, there is no clear trend with respect to the CO oxidation cycle history, i.e. no consistent increase or decrease with increasing cycle number. Thus, the near-ambient temperature region is the most informative, and here the amount of surface Pd is consistently higher for the core levels recorded before starting a cycle than at the end of a cycle. This shows that CO pulls Pd to the surface at ambient temperatures. CO-induced segregation of Pd has previously been predicted through DFT calculation for Pd-Ag surfaces [3]. Fernandes et al. [33] reported that the smaller relative spectral intensity of the CO-induced peak in the Pd $3d_{5/2}$ core level was smaller for $Pd_{75\%}Ag_{25\%}(100)$ at 35 °C in comparison to Pd (100) at 80 °C, and discussed how the results inferred Ag in the surface.

The profiles in Fig. 6 show a relatively strong decrease in CO bonded to Pd with increasing temperature, and then a more moderate increase as the CO coverage increases again upon lowering the temperature. Correspondingly, the amount of CO bound to Pd displayed in Fig. 7 is higher at the start of each cycle in comparison to the end. This signifies a higher level of Ag in the 1–2 topmost layers at the end of each cycle and testifies again to combined effects of coverage and segregation kinetics

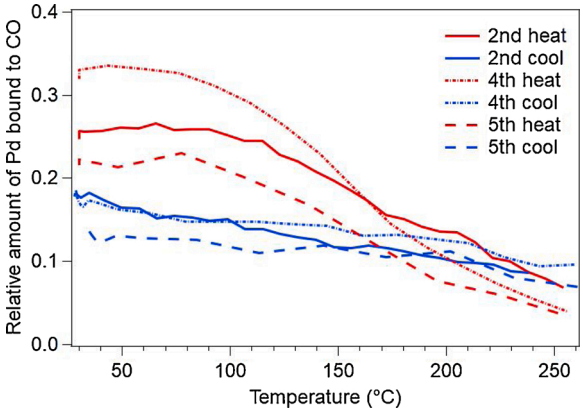

Fig. 6. Relative amount of Pd bound to CO in comparison to the total amount of Ag and Pd in the probed layers during CO oxidation over $Pd_{75\%}Ag_{25\%}(100)$ as function of sample temperature, for the 2nd (0.1 °C/s), 4th (0.2 °C/s) and 5th (0.4 °C/s) cycles. O_2:CO=10:1 and ~1.1 mbar total pressure.

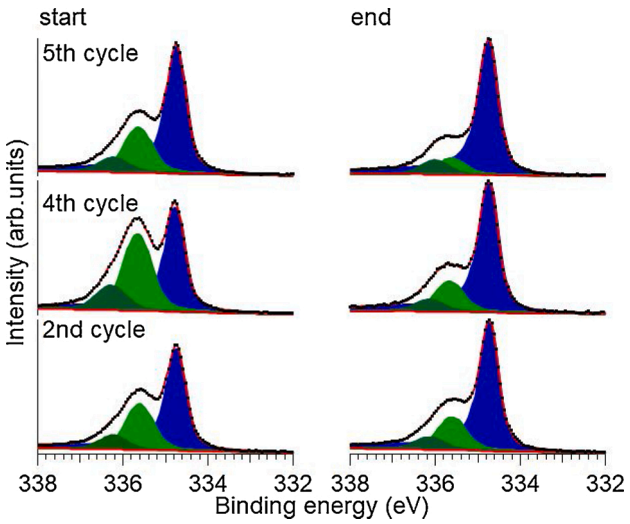

Fig. 7. Pd $3d_{5/2}$ core levels acquired at room temperature right before (left) and after (right) the 2nd, 4th and 5th CO oxidation cycles over $Pd_{75\%}Ag_{25\%}(100)$. The spectra were measured using a photon energy of 450 eV, O_2:CO=10:1 and ~1.1 mbar total pressure.

that moderates the segregation of Pd towards the surface upon cooling.

For all the cycles in Fig. 6 the relative amounts in the cooling cycle are relatively close in value, whereas there are larger differences between the heating sections of the cycles. Regardless of the amount of surface Pd at the beginning of a cycle, the values at the end of the cycle indicates a surface with more similar levels of surface Pd as the previous cycles. This is also reflected in Fig. 7 where the relative weight of CO bonded to Pd is similar for the spectra at the end of each cycle. The previous work of Fernandes et al. [33] on CO oxidation over $Pd_{75\%}Ag_{25\%}(100)$ suggested, based on theoretical calculations and comparisons between Pd 3d and Ag 3d before and after a cycle, that although the adsorbate coverage increased upon a reduction in temperature, there might be kinetic limitations for obtaining a Pd rich surface. In contrast, and analogous to the segregation within all the probed layers (Fig. 5), Figs. 6 and 7 infer that the segregation kinetics are relatively facile within the topmost layers and that the coverage effects actually control the termination.

There is a difference in the spectral weight of the Pd bound to CO between the end of the 4th cycle and the beginning of the 5th cycle (Fig. 7). The time between the sample reached room temperature at the end of the 4th cycle and the start of the temperature ramp in the 5th cycle was approximately 80 min. This result infers that there is an enrichment of Pd in the surface, hence appreciable segregation kinetics at ambient temperature. Spronsen et al. [62] also found through NAP-XPS exposure of Ag/PdAg/Ag(111) islands to ~0.7 mbar CO at ambient temperature induced migration of Pd towards the surface.

The time residing between cycles was not systematically varied, and the time window between the end of the 3rd and start of the 4th temperature cycle was approximately 60 min. Although this is shorter than between the 4th and 5th cycles, a largest relative amount of Pd in the surface was found for the start of the 4th cycle. Hence, there are additional factors that affect the amount of Pd in the surface than time of exposure to adsorbates at temperatures below 250 °C. The segregation kinetics in the topmost layers could be more facile than segregation deep within the bulk, yielding overall more exchange between Pd and Ag in the near-surface region during the cycling to 600 °C than to 450 °C.

4. Conclusion

The segregation behaviour of a $Pd_{75\%}Ag_{25\%}(100)$ single crystal during CO oxidation in oxygen rich conditions at a total pressure of 1.1 mbar was investigated using a combination of quadrupole mass spectrometry and near-ambient pressure x-ray photoelectron spectroscopy. Throughout six CO oxidation cycles with different heating rates and maximum temperatures of 450 °C or 600 °C we observe dynamic changes in the surface composition during reaction. The CO_2 formation hysteresis curves observed upon subsequent heating and cooling ramps were found to depend on initial conditions, heating rate and maximum heating temperature. After initial oxidation of the surface that leaves a rather thick Pd-oxide, a normal hysteresis curve in the CO_2 formation is observed, consistent with a practically Pd terminated surface. Reversed hysteresis is obtained in the following cycles upon heating to 450 °C in agreement with previous work. The CO_2 formation profile considerably changes upon heating to 600 °C, first displaying a prominent reversed hysteresis and thereafter very similar temperature dependency during heating and cooling, and less impact of mass transfer limitations.

By following the Ag $3d_{5/2}$ and Pd $3d_{5/2}$ core levels we show that it is possible to monitor cyclic segregation behaviour in Pd-Ag alloy surfaces, where the amount of Pd in the surface decreases upon heating under CO and O_2 gas mixtures. The segregation behaviour is reversed upon cooling. Assessment of the relative amount of Pd-to-total-metal captures some of the segregation behaviour but is insufficient with respect to revealing the changes in composition dynamics of the topmost 1–2 layers that clearly affect the reaction. Additional information could be extracted by quantifying the contribution to the Pd $3d_{5/2}$ core level that originates from CO bound to Pd. The spectra obtained while residing 60–80 min at ambient temperature revealed discernible kinetics of the Pd segregation to the topmost surface layer at these conditions, evident by the observed build-up of CO and consistent with more Pd slowly being pulled to the topmost surface layer.

CRediT authorship contribution statement

Marie D. Strømsheim: Methodology, Validation, Formal analysis, Investigation, Writing - original draft, Writing - review & editing, Visualization. **Ingeborg-Helene Svenum:** Conceptualization, Methodology, Validation, Formal analysis, Investigation, Data curation, Writing - original draft, Writing - review & editing, Visualization, Supervision, Funding acquisition. **Mehdi Mahmoodinia:** Investigation, Supervision. **Virgínia Boix:** Investigation, Writing - original draft, Writing - review & editing, Visualization. **Jan Knudsen:** Methodology, Validation, Investigation, Writing - original draft, Writing - review & editing, Supervision. **Hilde J. Venvik:** Conceptualization, Methodology, Investigation, Writing - review & editing, Visualization, Supervision, Project administration, Funding acquisition.

Declaration of Competing Interest

The authors declare that they have no known competing financial interests or personal relationships that could have appeared to influence the work reported in this paper.

Acknowledgments

This project is funded by the Research Council of Norway, project number 280903 (H_2MemX – Enabling ultrathin Pd based membranes through surface chemistry diagnostics and control). Virgínia Boix and Jan Knudsen acknowledge financial support from the Swedish Research Council (grant number 2017-04840). We acknowledge MAX IV Laboratory for time on Beamline HIPPIE under Proposal 20180307. Research conducted at MAX IV, a Swedish national user facility, is supported by the Swedish Research council under contract 2018-07152, the Swedish Governmental Agency for Innovation Systems under contract 2018-04969, and Formas under contract 2019-02496. We gratefully acknowledge the assistance of MAX IV Laboratory staff, in particularly Dr. Andrey Shavorskiy and Dr. Suyun Zhu of the HIPPIE beamline.

Appendix A. Supplementary data

Supplementary material related to this article can be found, in the online version, at doi:https://doi.org/10.1016/j.cattod.2021.02.007.

References

[1] K. McCullough, T. Williams, K. Mingle, P. Jamshidi, J. Lauterbach, High-throughput experimentation meets artificial intelligence: A new pathway to catalyst discovery, Phys. Chem. Chem. Phys. 22 (2020) 11174–11196, https://doi.org/10.1039/d0cp00972e.

[2] J.K. Nørskov, T. Bligaard, J. Rossmeisl, C.H. Christensen, Towards the computational design of solid catalysts, Nat. Chem. 1 (2009) 37–46, https://doi.org/10.1038/nchem.121.

[3] I.-H. Svenum, J.A. Herron, M. Mavrikakis, H.J. Venvik, Adsorbate-induced segregation in a PdAg membrane model system: Pd3Ag(1 1 1), Catal. Today 193 (2012) 111–119, https://doi.org/10.1016/j.cattod.2012.01.007.

[4] O.M. Løvvik, S.M. Opalka, Reversed surface segregation in palladium-silver alloys due to hydrogen adsorption, Surf. Sci. 602 (2008) 2840–2844, https://doi.org/10.1016/J.SUSC.2008.07.016.

[5] J. Greeley, M. Mavrikakis, Alloy catalysts designed from first principles, Nat. Mater. 3 (2004) 810–815, https://doi.org/10.1038/nmat1223.

[6] A.V. Ruban, H.L. Skriver, J.K. Nørskov, Surface segregation energies in transition-metal alloys, Phys. Rev. B - Condens. Matter Mater. Phys. 59 (1999) 15990–16000, https://doi.org/10.1103/PhysRevB.59.15990.

[7] M. Salmeron, R. Schlögl, Ambient pressure photoelectron spectroscopy: a new tool for surface science and nanotechnology, Surf. Sci. Rep. 63 (2008) 169–199, https://doi.org/10.1016/j.surfrep.2008.01.001.

[8] J. Schnadt, J. Knudsen, N. Johansson, Present and new frontiers in materials research by ambient pressure x-ray photoelectron spectroscopy, J. Phys. Condens. Matter 32 (2020) 413003, https://doi.org/10.1088/1361-648X/ab9565.

[9] C. Arble, M. Jia, J.T. Newberg, Lab-based ambient pressure X-ray photoelectron spectroscopy from past to present, Surf. Sci. Rep. 73 (2018) 37–57, https://doi.org/10.1016/j.surfrep.2018.02.002.

[10] P. Gélin, M. Primet, Complete oxidation of methane at low temperature over noble metal based catalysts: a review, Appl. Catal. B Environ. 39 (2002) 1–37, https://doi.org/10.1016/S0926-3373(02)00076-0.

[11] J.K. Ali, E.J. Newson, D.W.T. Rippin, Deactivation and regeneration of Pd-Ag membranes for dehydrogenation reactions, J. Memb. Sci. 89 (1994) 171–184, https://doi.org/10.1016/0376-7388(93)E0219-A.

[12] P.A. Sheth, M. Neurock, C.M. Smith, First-principles analysis of the effects of alloying Pd with Ag for the catalytic hydrogenation of acetylene-ethylene mixtures, J. Phys. Chem. B 109 (2005) 12449–12466, https://doi.org/10.1021/jp050194a.

[13] W.T. McGown, C. Kemball, D.A. Whan, M.S. Scurrell, Hydrogenation of acetylene in excess ethylene on an alumina supported palladium catalyst in a static system, J. Chem. Soc. Faraday Trans. 1 Phys. Chem. Condens. Phases. 73 (1977) 632–647, https://doi.org/10.1039/F19777300632.

[14] L. Xu, E.E. Stangland, M. Mavrikakis, Ethylene versus ethane: a DFT-based selectivity descriptor for efficient catalyst screening, J. Catal. 362 (2018) 18–24, https://doi.org/10.1016/j.jcat.2018.03.019.

[15] Q. Zhang, J. Li, X. Liu, Q. Zhu, Synergetic effect of Pd and Ag dispersed on Al2O3 in the selective hydrogenation of acetylene, Appl. Catal. A Gen. 197 (2000) 221–228, https://doi.org/10.1016/S0926-860X(99)00463-9.

[16] K. Atsonios, K.D. Panopoulos, A. Doukelis, A.K. Koumanakos, E. Kakaras, T. A. Peters, Y.C. van Delft, Introduction to palladium membrane technology. Palladium Membr. Technol. Hydrog. Prod. Carbon Capture Other Appl. Princ. Energy Prod. Other Appl., Elsevier Ltd, 2015, pp. 1–21, https://doi.org/10.1533/9781782422419.1.

[17] S. Zhang, Ö. Metin, D. Su, S. Sun, Monodisperse AgPd alloy nanoparticles and their superior catalysis for the dehydrogenation of formic acid, Angew. Chemie - Int. Ed. 52 (2013) 3681–3684, https://doi.org/10.1002/anie.201300276.

[18] F. Liao, T.W.B. Lo, S.C.E. Tsang, Recent developments in palladium-based bimetallic catalysts, Chem. Cat. Chem. 7 (2015) 1998–2014, https://doi.org/10.1002/cctc.201500245.

[19] G. Centi, Supported palladium catalysts in environmental catalytic technologies for gaseous emissions, J. Mol. Catal. A Chem. 173 (2001) 287–312, https://doi.org/10.1016/S1381-1169(01)00155-8.

[20] R.M. Heck, R.J. Farrauto, S.T. Gulati, Catalytic Air Pollution Control: Commercial Technology, 3rd ed., John Wiley & Sons, Inc., Hoboken, NJ, USA, 2009.

[21] M. Todorova, E. Lundgren, V. Blum, A. Mikkelsen, S. Gray, J. Gustafson, M. Borg, J. Rogal, K. Reuter, J.N. Andersen, M. Scheffler, The Pd(100)–($\sqrt{5}\times\sqrt{5}$)R27°-O surface oxide revisited, Surf. Sci. 541 (2003) 101–112, https://doi.org/10.1016/S0039-6028(03)00873-2.

[22] P. Kostelník, N. Seriani, G. Kresse, A. Mikkelsen, E. Lundgren, V. Blum, T. Šikola, P. Varga, M. Schmid, The surface oxide: a LEED, DFT and STM study, Surf. Sci. 601 (2007) 1574–1581, https://doi.org/10.1016/j.susc.2007.01.026.

[23] R. Toyoshima, M. Yoshida, Y. Monya, K. Suzuki, B.S. Mun, K. Amemiya, K. Mase, H. Kondoh, Active surface oxygen for catalytic CO oxidation on Pd(100) proceeding under near ambient pressure conditions, J. Phys. Chem. Lett. 3 (2012) 3182–3187, https://doi.org/10.1021/jz301404n.

[24] S. Blomberg, M.J. Hoffmann, J. Gustafson, N.M. Martin, V.R. Fernandes, A. Borg, Z. Liu, R. Chang, S. Matera, K. Reuter, E. Lundgren, In situ x-ray photoelectron spectroscopy of model catalysts: at the edge of the gap, Phys. Rev. Lett. 110 (2013) 117601, https://doi.org/10.1103/PhysRevLett.110.117601.

[25] B.L.M. Hendriksen, S.C. Bobaru, J.W.M. Frenken, Oscillatory CO oxidation on Pd(1 0 0) studied with in situ scanning tunneling microscopy, Surf. Sci. 552 (2004) 229–242, https://doi.org/10.1016/j.susc.2004.01.025.

[26] B.L.M. Hendriksen, M.D. Ackermann, R. van Rijn, D. Stoltz, I. Popa, O. Balmes, A. Resta, D. Wermeille, R. Felici, S. Ferrer, F.W. M, The role of steps in surface catalysis and reaction oscillations, Nat. Chem. 2 (2010) 730–734, https://doi.org/10.1038/nchem.728.

[27] R. van Rijn, O. Balmes, A. Resta, D. Wermeille, R. Westerström, J. Gustafson, R. Felici, E. Lundgren, J.W.M. Frenken, Surface structure and reactivity of Pd(100) during CO oxidation near ambient pressures, Phys. Chem. Chem. Phys. 13 (2011) 13167, https://doi.org/10.1039/c1cp20989b.

[28] M. Shipilin, J. Gustafson, C. Zhang, L.R. Merte, A. Stierle, U. Hejral, U. Ruett, O. Gutowski, M. Skoglundh, P.-A. Carlsson, E. Lundgren, Transient Structures of PdO during CO Oxidation over Pd(100), J. Phys. Chem. C. 119 (2015) 15469–15476, https://doi.org/10.1021/acs.jpcc.5b04400.

[29] R. Westerström, M.E. Messing, S. Blomberg, A. Hellman, H. Grönbeck, J. Gustafson, N.M. Martin, O. Balmes, R. van Rijn, J.N. Andersen, K. Deppert, H. Bluhm, Z. Liu, M.E. Grass, M. Hävecker, E. Lundgren, Oxidation and reduction of Pd(100) and aerosol-deposited Pd nanoparticles, Phys. Rev. B 83 (2011) 115440, https://doi.org/10.1103/PhysRevB.83.115440.

[30] M. Chen, X.V. Wang, L. Zhang, Z. Tang, H. Wan, Active surfaces for CO oxidation on palladium in the hyperactive state, Langmuir 26 (2010) 18113–18118, https://doi.org/10.1021/la103140w.

[31] T.C.R. Rocha, A. Oestereich, D.V. Demidov, M. Hävecker, S. Zafeiratos, G. Weinberg, V.I. Bukhtiyarov, A. Knop-Gericke, R. Schlögl, The silver-oxygen system in catalysis: new insights by near ambient pressure X-ray photoelectron spectroscopy, Phys. Chem. Chem. Phys. 14 (2012) 4554–4564, https://doi.org/10.1039/c2cp22472k.

[32] N. Vicinanza, I.-H. Svenum, L.N. Næss, T.A. Peters, R. Bredesen, A. Borg, H. J. Venvik, Thickness dependent effects of solubility and surface phenomena on the hydrogen transport properties of sputtered Pd77%Ag23% thin film membranes, J. Memb. Sci. 476 (2015) 602–608, https://doi.org/10.1016/J.MEMSCI.2014.11.031.

[33] V.R. Fernandes, M. Van Den Bossche, J. Knudsen, M.H. Farstad, J. Gustafson, H. J. Venvik, H. Grönbeck, A. Borg, Reversed hysteresis during CO oxidation over Pd75Ag25(100), ACS Catal. 6 (2016) 4154–4161, https://doi.org/10.1021/acscatal.6b00658.

[34] M.D. Strømsheim, J. Knudsen, M.H. Farstad, L. Sørvik, X. Guo, H.J. Venvik, A. Borg, Near ambient pressure XPS investigation of CO oxidation over Pd3Au (100), Top. Catal. 60 (2017) 1439–1448, https://doi.org/10.1007/s11244-017-0831-z.

[35] L.E. Walle, H. Grönbeck, V.R. Fernandes, S. Blomberg, M.H. Farstad, K. Schulte, J. Gustafson, J.N. Andersen, E. Lundgren, A. Borg, Surface composition of clean and oxidized Pd75Ag25(100) from photoelectron spectroscopy and density functional theory calculations, Surf. Sci. 606 (2012) 1777–1782, https://doi.org/10.1016/j.susc.2012.07.006.

[36] P.T. Wouda, M. Schmid, B.E. Nieuwenhuys, P. Varga, Adsorbate Migration on PdAg (111), 1999, https://doi.org/10.1016/S0039-6028(98)00937-6.

[37] T. Marten, O. Hellman, A.V. Ruban, W. Olovsson, C. Kramer, J.P. Godowski, L. Bech, Z. Li, J. Onsgaard, I.A. Abrikosov, Double-segregation effect in Agx Pd1-x /Ru (0001) thin film nanostructures, Phys. Rev. B - Condens. Matter Mater. Phys. 77 (2008) 125406, https://doi.org/10.1103/PhysRevB.77.125406.

[38] L. Vitos, A.V. Ruban, H.L. Skriver, J. Kollár, The surface energy of metals, Surf. Sci. 411 (1998) 186–202, https://doi.org/10.1016/S0039-6028(98)00363-X.

[39] J. Shu, B.E.W. Bongondo, B.P.A. Grandjean, A. Adnot, S. Kaliaguine, Surface segregation of PdAg membranes upon hydrogen permeation, Surf. Sci. 291 (1993) 129–138, https://doi.org/10.1016/0039-6028(93)91484-7.

[40] J. Knudsen, J.N. Andersen, J. Schnadt, A versatile instrument for ambient pressure x-ray photoelectron spectroscopy: the Lund cell approach, Surf. Sci. 646 (2016) 160–169, https://doi.org/10.1016/j.susc.2015.10.038.

[41] H. Bluhm, M. Hävecker, A. Knop-Gericke, M. Kiskinova, R. Schlögl, M. Salmeron, In situ X-ray photoelectron spectroscopy studies of gas-solid interfaces at near-ambient conditions, MRS Bull. 32 (2007) 1022–1030, https://doi.org/10.1557/mrs2007.211.

[42] S. Tougaard, QUASES-IMFP-TPP2M, (n.d.). http://www.quases.com/products/quases-imfp-tpp2m/.

[43] S. Tanuma, C.J. Powell, D.R. Penn, Calculations of electron inelastic mean free paths. V. Data for 14 organic compounds over the 50-2000 eV range, Surf. Interface Anal. 21 (1994) 165–176, https://doi.org/10.1002/sia.740210302.

[44] C.J. Powell, Practical guide for inelastic mean free paths, effective attenuation lengths, mean escape depths, and information depths in x-ray photoelectron spectroscopy, J. Vac. Sci. Technol. A 38 (2020), 023209, https://doi.org/10.1116/1.5141079.

[45] S. Doniach, M. Sunjic, Many-electron singularity in X-ray photoemission and X-ray line spectra from metals, J. Phys. C Solid State Phys. 3 (1970) 285–291, https://doi.org/10.1088/0022-3719/3/2/010.

[46] V.R. Fernandes, J. Gustafson, M.H. Farstad, L.E. Walle, S. Blomberg, E. Lundgren, H.J. Venvik, A. Borg, H2 reduction of surface oxides on Pd-based membrane model systems – the case of Pd(100) and Pd75Ag25(100), Appl. Surf. Sci. 313 (2014) 794–803, https://doi.org/10.1016/j.apsusc.2014.06.077.

[47] S. Blomberg, J. Zetterberg, J. Gustafson, J. Zhou, C. Brackmann, E. Lundgren, Comparison of AP-XPS and PLIF measurements during CO oxidation over Pd single crystals, Top. Catal. 59 (2016) 478–486, https://doi.org/10.1007/s11244-015-0524-4.

[48] J.J. Yeh, I. Lindau, Atomic subshell photoionization cross sections and asymmetry parameters: 1 ⩽ Z ⩽ 103, At. Data Nucl. Data Tables. 32 (1985) 1–155, https://doi.org/10.1016/0092-640X(85)90016-6.
[49] I. WaveMetrics, Igor Pro, (n.d.). https://www.wavemetrics.com/.
[50] J. Andersen, M. Qvarford, R. Nyholm, S. Sorensen, C. Wigren, Surface core-level shifts as a probe of the local overlayer structure: CO on Pd(100), Phys. Rev. Lett. 67 (1991) 2822–2825, https://doi.org/10.1103/PhysRevLett.67.2822.
[51] P. Uvdal, P.A. Karlsson, C. Nyberg, S. Andersson, N.V. Richardson, On the structure of dense CO overlayers, Surf. Sci. 202 (1988) 167–182, https://doi.org/10.1016/0039-6028(88)90067-2.
[52] A.R. Head, O. Karslıoğlu, T. Gerber, Y. Yu, L. Trotochaud, J. Raso, P. Kerger, H. Bluhm, CO adsorption on Pd(100) studied by multimodal ambient pressure X-ray photoelectron and infrared reflection absorption spectroscopies, Surf. Sci. 665 (2017) 51–55, https://doi.org/10.1016/j.susc.2017.08.009.
[53] R. Toyoshima, N. Hiramatsu, M. Yoshida, K. Amemiya, K. Mase, B.S. Mun, H. Kondoh, CO adsorption on Pd–Au alloy surface: reversible adsorption site switching induced by high-pressure CO, J. Phys. Chem. C. 120 (2016) 416–421, https://doi.org/10.1021/acs.jpcc.5b10661.
[54] N.J. Firet, M.A. Blommaert, T. Burdyny, A. Venugopal, D. Bohra, A. Longo, W. A. Smith, Operando EXAFS study reveals presence of oxygen in oxide-derived silver catalysts for electrochemical CO 2 reduction, J. Mater. Chem. A 7 (2019) 2597–2607, https://doi.org/10.1039/c8ta10412c.
[55] H. Zhong, M. Iguchi, M. Chatterjee, Y. Himeda, Q. Xu, H. Kawanami, Formic acid-based liquid organic hydrogen carrier system with heterogeneous catalysts, Adv. Sustain. Syst. 2 (2018) 1700161, https://doi.org/10.1002/adsu.201700161.
[56] N.A. Khan, A. Uhl, S. Shaikhutdinov, H.-J. Freund, Alumina supported model Pd–Ag catalysts: a combined STM, XPS, TPD and IRAS study, Surf. Sci. 600 (2006) 1849–1853, https://doi.org/10.1016/j.susc.2006.02.016.
[57] Y. Soma-Noto, W.M.H. Sachtler, Infrared spectra of carbon monoxide adsorbed on supported palladium and palladium-silver alloys, J. Catal. 32 (1974) 315–324, https://doi.org/10.1016/0021-9517(74)90081-5.
[58] Y. Ma, T. Diemant, J. Bansmann, R.J. Behm, The interaction of CO with PdAg/Pd (111) surface alloys - A case study of ensemble effects on a bimetallic surface, Phys. Chem. Chem. Phys. 13 (2011) 10741–10754, https://doi.org/10.1039/c1cp00009h.
[59] G. McElhiney, H. Papp, J. Pritchard, The adsorption of Xe and CO on Ag(111), Surf. Sci. 54 (1976) 617–634, https://doi.org/10.1016/0039-6028(76)90209-0.
[60] A. Noordermeer, G.A. Kok, B.E. Nieuwenhuys, A comparative study of the behaviour of the PdAg(111) and Pd(111) surfaces towards the interaction with hydrogen and carbon monoxide, Surf. Sci. 165 (1986) 375–392, https://doi.org/10.1016/0039-6028(86)90814-9.
[61] V.R. Fernandes, J. Gustafson, I.-H. Svenum, M.H. Farstad, L.E. Walle, S. Blomberg, E. Lundgren, A. Borg, Reduction behavior of oxidized Pd(100) and Pd75Ag25(100) surfaces using CO, Surf. Sci. 621 (2014) 31–39, https://doi.org/10.1016/j.susc.2013.10.018.
[62] M.A. van Spronsen, K. Daunmu, C.R. O'Connor, T. Egle, H. Kersell, J. Oliver-Meseguer, M.B. Salmeron, R.J. Madix, P. Sautet, C.M. Friend, Dynamics of surface alloys: rearrangement of Pd/Ag(111) induced by CO and O 2, J. Phys. Chem. C. 123 (2019) 8312–8323, https://doi.org/10.1021/acs.jpcc.8b08849.